Springer

Journal of Mechanical Science and Technology 22 (2008) 1734~1746

Journal of Mechanical Science and Technology

www.springerlink.com/content/1738-494x
DOI 10.1007/s12206-008-0317-9

Design and fabrication of a scanning electron microscope using a finite element analysis for electron optical system

Man-Jin Park[1], Dong Hwan Kim[2], Keun Park[2], Dong Young Jang[3] and Dong-Chul Han[4,*]

[1]*School of Mechanical and Aerospace Engineering, Seoul National University, Shinlim-Dong San 56-1, Seoul 151-742, Korea*
[2]*School of Mechanical Design and Automation Engineering, Seoul National University of Technology, 172 Gongreung-dong, Nowon-gu, Seoul 139-743, Korea*
[3]*Department of Industrial Information and System Engineering, Seoul National University of Technology, 172 Gongreung-dong, Nowon-gu, Seoul 139-743, Korea*
[4]*School of Mechanical and Aerospace Engineering, Seoul National University, Shinlim-Dong San 56-1, Seoul 151-742, Korea*

(Manuscript Received December 28, 2007; Revised March 24, 2008; Accepted March 26, 2008)

Abstract

In this paper, we describe the design and fabrication of a thermionic scanning electron microscope (SEM) and examine its characteristics analytically. In the design process, the dimensions and capacity of the SEM components, such as the electron column, lenses, and apertures, were determined using finite element analysis. All components were integrated systematically during fabrication in order to achieve the maximum performance by adjusting the lens parameters, high voltage source, and image calibration methods. As a result, a thermionic SEM image with high resolution was achieved. We discuss the primary considerations required to achieve a high-performance image.

Keywords: Scanning electron microscope; Thermal emission; Electromagnetic lens; Finite element analysis

1. Introduction

With recent advances in nanotechnology, various pieces of measurement and analysis equipment have become indispensable for measuring nanoscale objects. Successful research in nanotechnology depends on high-performance measurement or analysis equipment; therefore, the development of such equipment is of great importance. In particular, the scanning electron microscope (SEM) is an important tool used to observe surfaces and analyze nanoscale material components.

The history of electron microscopy began with the development of electron optics [1]. In 1926, Busch studied the trajectories of charged particles in axially symmetric electric and magnetic fields, and laid the foundation for geometrical electron optics when he showed that such fields could act as particle lenses. Nearly at the same time, the French physicist de Broglie introduced the concept of electron waves. A frequency and hence a wavelength was associated with charged particles: this marked the beginning of wave-electron optics. Following these two discoveries in electron optics, the idea of an electron microscope began to take shape [1].

SEMs can be classified into two groups: thermionic and field emission. A field emission SEM has the highest magnification capability and is widely used in industries and research [2-4]. However, field emission SEMs are extremely expensive and require a high level of precautions, including an ultra high vacuum and a clean room, compared to thermionic SEMs. The need for SEMs in the semiconductor industry continues to increase. However, the measurements are a slow process as the SEM scans the object using an

*Corresponding author. Tel.: +82 2 880 7139, Fax.: +82 2 883 1513
E-mail address: dchan@amed.snu.ac.kr

electron beam. To eliminate this drawback, a miniature and potentially portable SEM with small column dimensions or a multiple column arrangement has been developed [5, 6], but it suffers from poor resolution.

SEMs use extremely short wavelengths (smaller than the wavelength of visible light) to enhance the resolution. Compared to an optical microscope that uses a visible light source with a wavelength of 300 to 700 nm, SEMs use an electron source with a wavelength of 1 nm. The structure and principle of SEMs are similar to optical microscopes. Optical lenses for focusing light in optical microscopes are substituted by electromagnetic lenses for focusing electron beams in SEMs. The electromagnetic lenses cause the electron beam to focus or diverge, depending on the electric current applied on the coils.

In this article, we describe the design and fabrication of a thermionic compact SEM with better performance in terms of resolution and image stability. Our high-resolution SEM is user-controlled and operates using a monitor. Before designing our SEM, beam trajectory analyses in the SEM column were performed for various types of lenses and apertures using the OPERA-3D [7] software. These analyses provided guidelines that resulted in an efficient SEM. Optimal design aspects for various parameters, such as the number of apertures and their arrangement, the pole-piece design of the magnetic lenses, and the excitation current conditions for the magnetic lenses, were considered. We used the simulations to investigate the effect of these design parameters on the SEM performance.

2. System fabrication and experiments

A thermionic SEM consists of various mechanical and electrical parts, including an electron gun, a column, a stage, a chamber, electromagnetic lenses, and a controller generating an appropriate current in each coil. Fig. 1 shows a three-dimensional (3D) drawing of a thermal SEM. Fig. 2 illustrates all the components in the electron optical column of our developed SEM; each component was designed and placed to maximize the focusing capability and to enhance the resolution. It is evident from Fig. 2 that the SEM is not very large: the dimensions of the column and the chamber together are only $510 \times 460 \times 500$ mm. The following sections describe the development of the key components of our thermionic SEM.

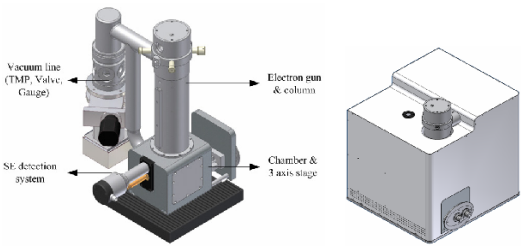

(a) Designed mini-SEM (b) Case surrounding the mini-SEM

Fig. 1. 3D image of our fabricated thermal SEM:

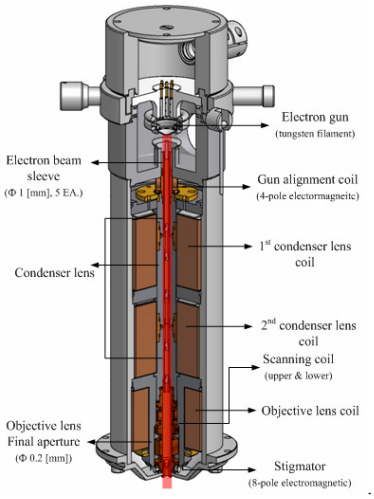

(a) Section view

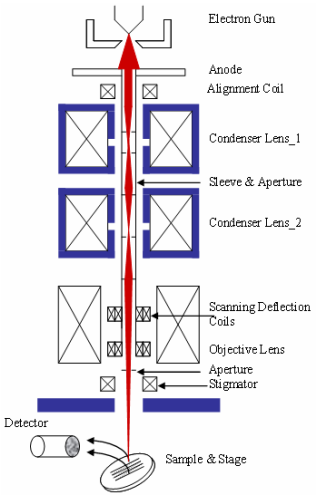

(b) Schematic diagram of the lens

Fig. 2. Assembled electron optical components (electron gun and electron optical column): (a) section view and (b) schematic diagram of the lenses.

2.1 Electron beam emission characteristics of thermal electron gun

The electron gun consisted of three electrodes: the cathode, Wehnelt cylinder, and anode. The cathode consisted of a tungsten wire filament bent in the shape of a hairpin with a diameter of 0.15 mm. It decreased the electron beam diameter to guarantee minimal electron emissions at the filament end point. This filament operated stably at 2700 K. The cathode had a low work function (4.5 eV) and high mechanical strength to ensure long-term operation. Tungsten cathodes are widely used because they are both reliable and inexpensive. The Wehnelt cylinder induced the electron beam production from the cathode. It was fabricated and tested many times to ensure the reliability and stability of the electron beam source. The anode was used to accelerate the electron beam after it left the cathode, induced by the Wehnelt cylinder.

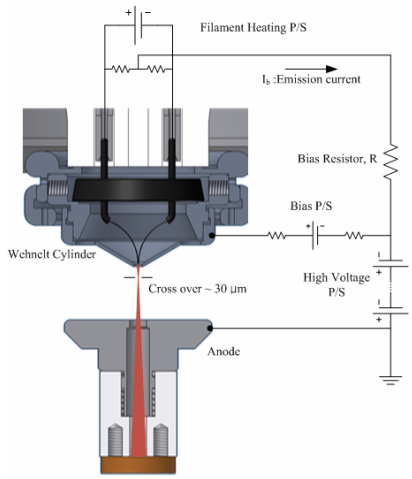

Fig. 3. Configuration of a thermionic emission gun.

In addition to a high-voltage source, the electrical power system consisted of three parts that helped with the emission of electrons by controlling the heating of the filament, induction of the cathode, and acceleration of the electron beam. When scanning the electron beam, the high voltages applied on the electrodes should be stable without severe voltage ripples. Our fabricated high-power source had ripples that were less than 10^{-3} % of the reference voltage. The voltages applied on the tungsten filament, cathode, and Wehnelt cylinder ranged from -5 to 25 kV, and the anode was electrically grounded. The electrons emitted from the filament produced a crossover at the Wehnelt, which was under a negative biased voltage in the range of 3 kV, as shown in Fig. 3. The electrons were subjected to a strong acceleration towards the anode due to this high voltage difference between the cathode and the anode. The accelerated electrons reached the specimen through subsequent focusing lenses built in the electron optical column.

A half-fixed biased gun was employed to maintain a high stability and beam current in the gun structure. Thermal emission experiments were performed in a specially manufactured vacuum chamber; the vacuum level inside the chamber was maintained under 10^{-5} torr. The emitted electron beam went into a narrow sleeve that functioned as a wave guide and was made of a conductive phosphorous copper. The emitted electron beam current, which passed through a 5 mm hole, was measured at a Faraday cup connected to an electrometer (Keithley 6517) that could measure picoampere-level current. The electron beam was

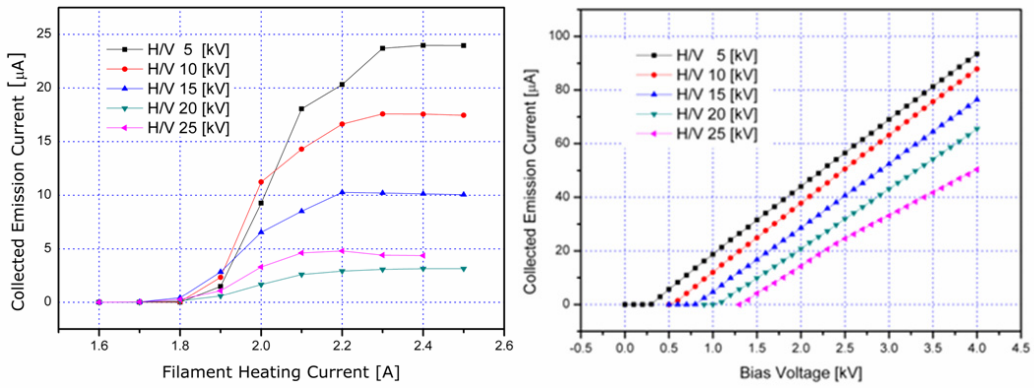

(a) Filament heating current (b) Bias voltage

Fig. 4. Variation in the electron emission current with the filament heating current and bias voltage.

aligned mechanically and electrically in the electron gun to measure the electron beam current at the Faraday cup. The beam emission currents were measured as shown in Fig. 4(a) by increasing the filament current from 1.6 through 2.6 A in steps of 0.1 A for five applied acceleration voltages (5, 10, 15, 20 and 25 kV). Around 2.3 A, the current reached a saturation point for all applied voltages. For each acceleration voltage, the changes in the emission current were also measured by changing the bias voltage; these results are illustrated in Fig. 4(b).

The emission current increased as a high bias voltage was imposed on the Wehnelt. Since the emission current and the bias voltage have a linear relationship, an appropriate bias voltage selection is recommended for a large electron beam.

The bias between the cathode and the Wehnelt is often produced by a simple feedback consisting of a resistor connected in series with the cathode. As the electron current emitted from the cathode increases, the cathode becomes more positive with respect to the Wehnelt so that the emitted current is stabilized. The preferred arrangement is to use an electric stabilizer circuit that monitors the beam current and alters the bias voltage to keep the current constant. The purpose of the Wehnelt electrode is to control the electric field close to the cathode so that electrons are emitted from only a small area of the cathode and are subsequently focused into a narrow beam suitable for further demagnification by a series of electron lenses to form the final electron probe. Normally such guns are designed and adjusted so that the electron beam is forced into a narrow "crossover spot" at a short distance beyond the anode, which is then demagnified to form the final probe.

2.2 Electromagnetic lenses

The lenses in a SEM play a vital role in demagnifying the electron beam to obtain a focused beam spot. A magnetic lens is most frequently used for narrowing the beam by driving a magnetic field-applied electric current on the coil[8]. By changing the coil current, the focal length can be adjusted, ensuring a highly focused beam. This magnetic flux causes the electron beam to deflect, which is explained by Lorenz's law. We used two condenser lenses and one objective lens to demagnify the electron beam spot size down to a few nanometers from the large crossover diameter at the Wehnelt cylinder in the electron gun. The condenser lenses, objective lens, and lens apertures were installed serially along the beam trajectory axis, yielding a successively more focused electron beam. The condenser lens, located right after the anode, functioned as a first focusing device for the electron beam, while the second condenser lens also focused the electron beam to demagnify it again. The smaller the beam spot size achieved by the combination of the condenser lenses, the higher the resolution. Once past the condenser lenses, the electron beam was further focused by the objective lens before finally striking the specimen. The aperture was a small hole made of a non-magnetic refractory metal. It intercepted the electrons that passed through the periphery of the lenses and allowed only electrons in the dominant part of the whole electron beam to pass through. Several apertures were placed in the center of the electron beam. The size of the last aperture was predominant in determining the beam size, brightness, diverging angle, and depth of focus. The smaller the last aperture, the higher the resolution. This, however, results in a small number of electrons on the specimen. Therefore, a precise modulation of the aperture is necessary. In our SEM, six apertures were employed to enhance the resolution. The efficiency of the magnetic field was maximized to improve the performance of the electromagnetic lenses. Since the magnetic field depends on the coil current and number of turns, the lens parameters, such as beam energy, width of coils, and inner and outer diameters of the coils, lens geometry, and design, were determined with special care. A strong magnetic field can be obtained inside and outside the lens by focusing the distributed magnetic field. A soft and pure iron material was employed to generate a strong magnetic field

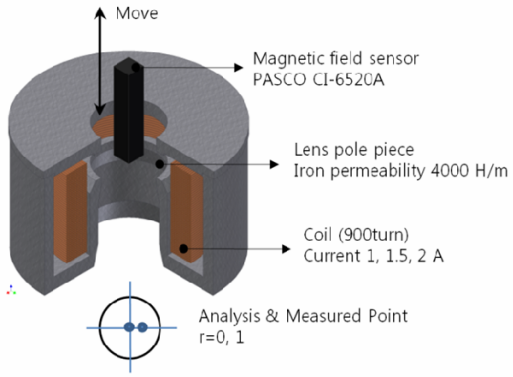

Fig. 5. Experimental system for measuring the magnetic field along the center of the lens.

in a specific area. The magnetic flux measurement device is shown in Fig. 5 while the flux measurement along the lens center is plotted in Fig. 6. Comparison between numerical analysis and experimental results showed a good agreement, which indicates that the lens design was effective.

Our electron optical system consisted three magnetic lenses: two condenser lenses and an objective lens. These magnetic lenses played an important role in deflecting the electron beams so as to focus them at a specific point. In order to predict the beam trajectory, the electromagnetic field originating from the magnetic lenses was calculated using a finite element analysis [9].

2.3 Controller design

The controller in our SEM controlled all components and monitored the signals from the driver. We used a user-friendly fully digital controller rather than a classical analog one. The controlled SEM components included the high-voltage source of 2 to 25 kV, lenses to focus the electron beam, vacuum system to maintain the high vacuum inside the column and the chamber, scan generator to scan the electron beam

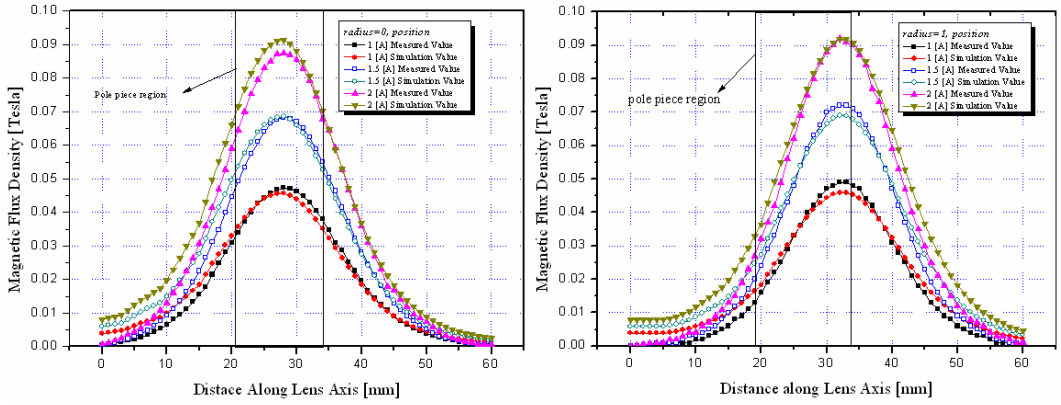

(a) Radius $r = 0$ (b) Radius $r = 1$

Fig. 6. Comparison of the magnetic flux density obtained from experiment and numerical analysis.

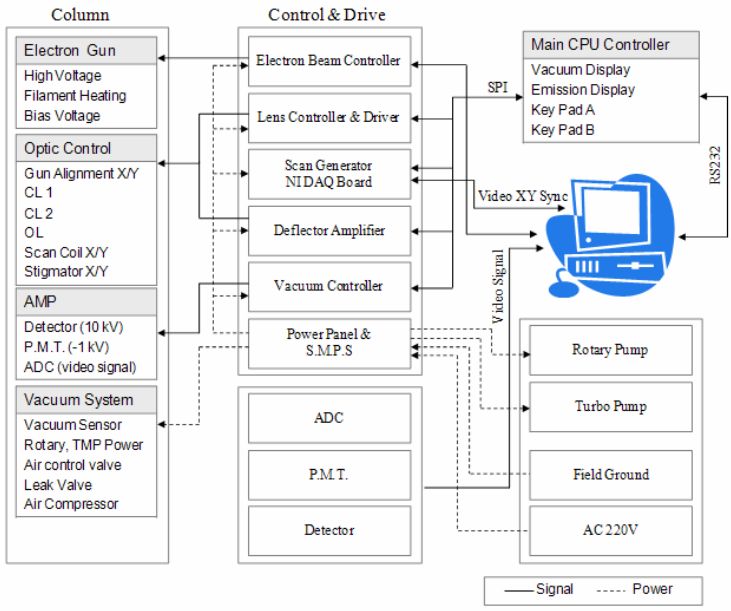

Fig. 7. Flow diagram of the SEM controller.

along the specimen, amplifier to amplify the detected secondary electrons, and analog-to-digital (AD) converter to convert the amplified signal into a digital signal. The control flow for this system is shown in Fig. 7.

The electron beam control was located on top of the controller and used to control the electron gun. The lens currents that generated the magnetic field flowed into the coils to focus the electron beam. The values of the desired digitized currents were received from the main microcontroller, which was also connected to the main personal computer (PC) using a RS232 serial port. The scan generator that received synchronized video x and y-axis signals from the PC scanned the electron beam by sending signals to the lens controller and the deflection amplifier to set a certain magnification value. As the desired magnification value was obtained, the focused electron beam scanned the specimen, emitting numerous secondary electrons. Fig. 8 shows a diagram of the secondary electron detector. The emitted electrons were detected by a sensor located at the pre-amplification stage and were later amplified by a photo multiplier tube (PMT). This signal was digitally converted and fed into a universal serial bus (USB) data acquisition (DAQ) board (NI-6251, National Instruments) installed in the PC. The PC processed the acquired image signal and finally transmitted the image result to the monitor. The vacuum sensor and valve sensor checked the status of the chamber so that the vacuum value could also be displayed. The main digital signal processing (DSP) board controlled each controller, received the keypad input, and displayed the current value. The switching mode power supply (SMPS) supplied power to each controller while the power panel supplied electric power to the rotary pump, turbo pump, and leak valve.

3. Finite element analysis of the electron optical system

To design an efficient SEM system, we used finite element analysis[9] to identify the optimal design criteria for focusing the beam under a magnetic field, encompassing the lenses, apertures, and electron beam source. The fabrication of our SEM was primarily based on this analysis, which suggested guidelines for the dimensions of each component and locations for those components inside the SEM. Precise measurements of the electron beam characteristics, such as spot size and density, cannot be easily obtained in a real SEM due to the limitations of the sensors installed inside it. Through this analysis, we demonstrated that the dimensions of the SEM components and their placement strongly affected the SEM resolution. Thus, a SEM design can be optimized using this numerical analysis. The finite element analysis indirectly demonstrated that the magnetic flux and electron beam deflection were dependent solely on the current on the coil.

Expensive equipment or special sensors to measure the physical quantities are not required when using simulated results. The theory and finite element analysis used to investigate the beam trajectory and focusing using various design parameters for the SEM components are described in the following sections.

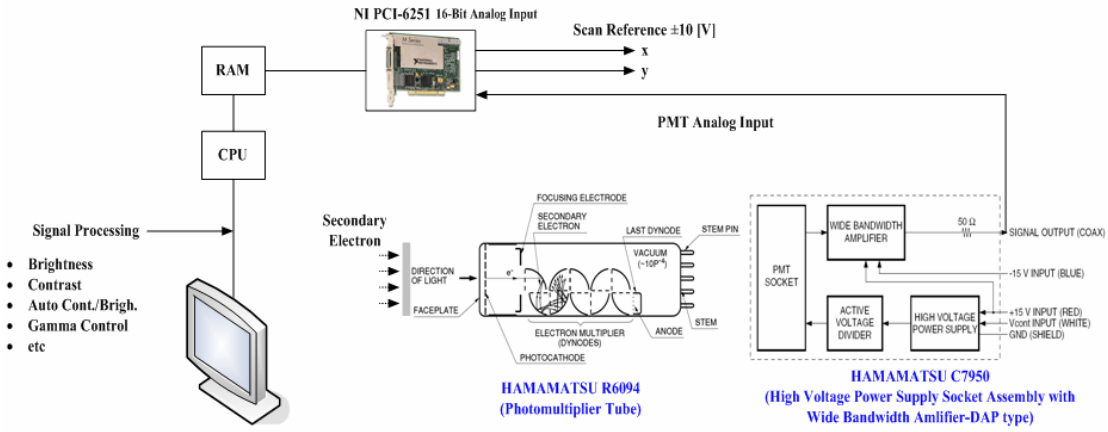

Fig. 8. Secondary electron collection and signal amplification.

3.1 Electron gun analysis

We simulated the gun structure as shown in Fig. 9. The gun consisted of a hair-pin emitter, a Wehnelt cylinder, an anode, a sleeve, and a Faraday cup. Electrons were accelerated to about -15 kV by the anode potential. In the simulation, the Wehnelt cylinder voltage was set to -15 kV [-70 to +40 V], the Wehnelt cylinder hole diameter was 1.5 mm, the distance between the emitter and Wehnelt cylinder was 1 mm, and the distance between the Wehnelt cylinder and the anode was 5 mm. Along the route from the emitter to the anode, the paths of the individual electrons crossover. The real source in an electron gun is projected onto the specimen surface to generate an image. The condenser and objective lenses then produce a demagnified image of the crossover on the specimen by subsequent focusing.

The electron beam emitted from the filament forms a crossover at a specific point as a function of the negative bias voltage applied on the Wehnelt cylinder. Therefore, a simulation was performed to determine the emission characteristics, including spot size and emission current, as a function of the bias voltage. The results are illustrated in Fig. 10(a) and (b). In both cases, the bias voltage was changed from -70 V to 40 V at an increment of 10 V. The spot size increased linearly with the value of the bias voltage, as shown in Fig. 10(a). However, the emission current detected at the collector decreased with increasing bias voltage. This indicates that the emitted electrons formed the crossover as a function of the applied bias voltage, which can be used to control the dispersion

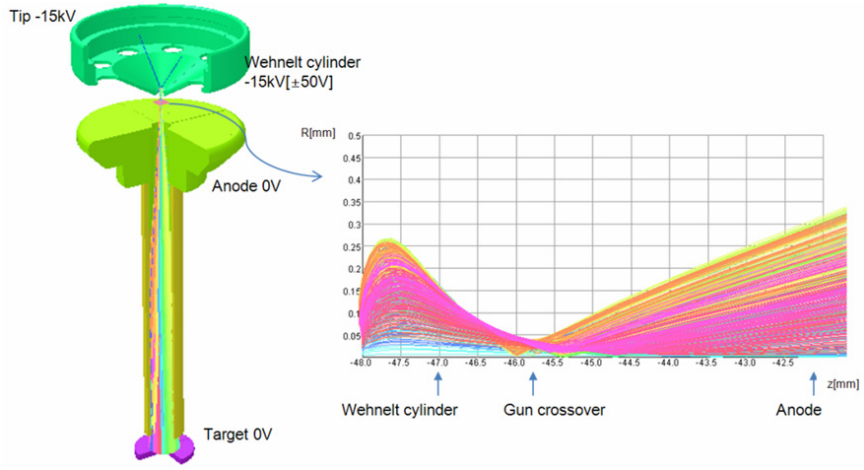

Fig. 9. Gun structure and simulated electron beam trajectories.

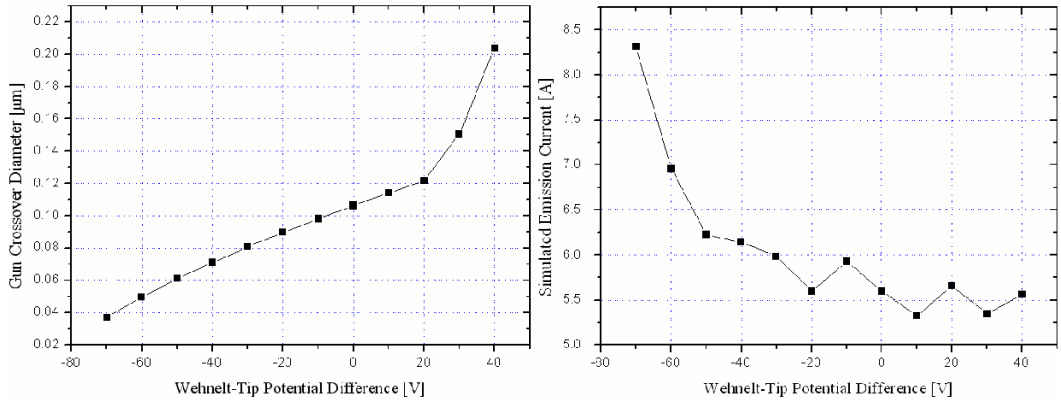

(a) Crossover diameter (b) Emission current

Fig. 10. (a) Crossover diameter and (b) emission current as a function of the negative bias voltage applied on the Wehnelt cylinder.

angle. The minimum crossover and the highest emission current were 36 μm and 8.3 μA, respectively, at a bias voltage of -70 V.

The variation in the beam spot radius as a function of the axial distance is shown in Fig. 11. The bias voltage was set to -70 V. The minimum spot radius at the crossover position, approximately 2.3 mm from the Wehnelt, was 0.06 mm.

If the round tip of the electron gun is rotationally symmetric, it can provide a good test of the significance of the details in the emission modeling. The spot size and crossover position on the optical system are critical for this application.

3.2 Electro-magnetic field analysis of the lens system

The electromagnetic lens characteristics were also analyzed by a finite element analysis. The validity of this approach was demonstrated by experiments. In general, the pole piece gap in the magnetic lens is designed to be as small as possible to increase the magnetic flux intensity. This, however, makes it difficult to measure the magnetic flux. An experimental lens was designed and fabricated to resolve this issue. A schematic diagram for the lens is depicted in Fig. 5.

Considering the axisymmetric properties of the lens, an electromagnetic analysis was performed using OPERA 3D based on a 3D axisymmetric shape. The magnetic flux generated from the coil easily penetrated the relatively high-permeable pure iron and was concentrated near the pole piece. To measure the effect quantitatively, the magnetic fluxes B_z and B_r were measured as a function of distance from the lens center.

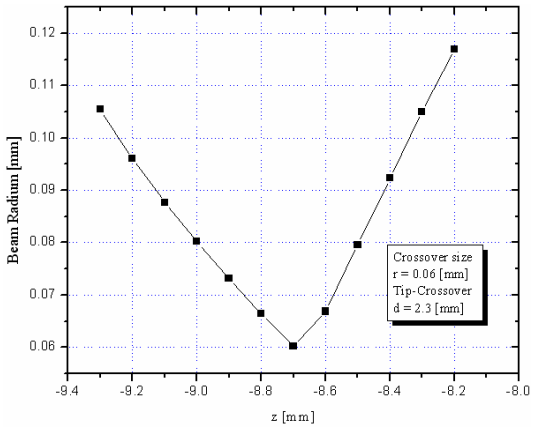

Fig. 11. Variation in the beam spot radius as a function of the axial distance.

From the (*B*-*H*) curve of pure iron, the permeability of the linear region of the curve was estimated as 4000 [H/m]. To compute the focal length of the condenser lens, the magnetic flux must be measured (or estimated by numerical analysis) exactly. The magnetic flux distributions near the pole piece were obtained from OPERA 3D/TOSCA, and the results are shown in Fig. 12.

Table 1 summarizes basic specifications of the coils and the corresponding current densities for the three magnetic lenses. The lenses were designed using axisymmetrical magnetic lenses with a gap width of 2 mm and diameter of 5 mm, and an unsymmetrical objective pole piece.

Fig. 12 shows the magnetic flux distributions around the two condenser lenses and the objective lens. Fig. 13 shows the magnetic flux distribution in the electron optical system. The magnetic flux for each lens is plotted as a vector plot under a given current condition. Most of the magnetic fields were distributed at the region of the pole piece. If the magnetic flux density did not exceed 2.0 Tesla, the column material could be magnetized. Except for the region around the lens, however, the magnetic flux of the housing material represented less than 1 Tesla. The direction of the applied current was the same as that of the magnetic flux. Thus, the magnitude of the magnetic flux around the pole piece acting as a lens represented the maximum value. On the contrary, the magnetic flux in the radial direction represented the minimum value. Based on this fact, the focal length of the electron beam had changed.

Therefore, lens characteristics can be driven by controlling both the coil current and the shape of the pole piece, and it is possible to determine the relationship between the applied current and pole piece shape.

Table 1. Basic specifications of coils for the three magnetic lenses.

Lens Type	No. of turns	Outer diameter (mm)	Inner diameter (mm)	Height (mm)	Current density (A/mm^2)
Condenser lens (1)	920	78	26	65	1.36 - 1.88
Condenser lens (2)	920	78	26	65	1.25 - 1.74
Objective lens	600	84	46	55	0.40 - 0.68

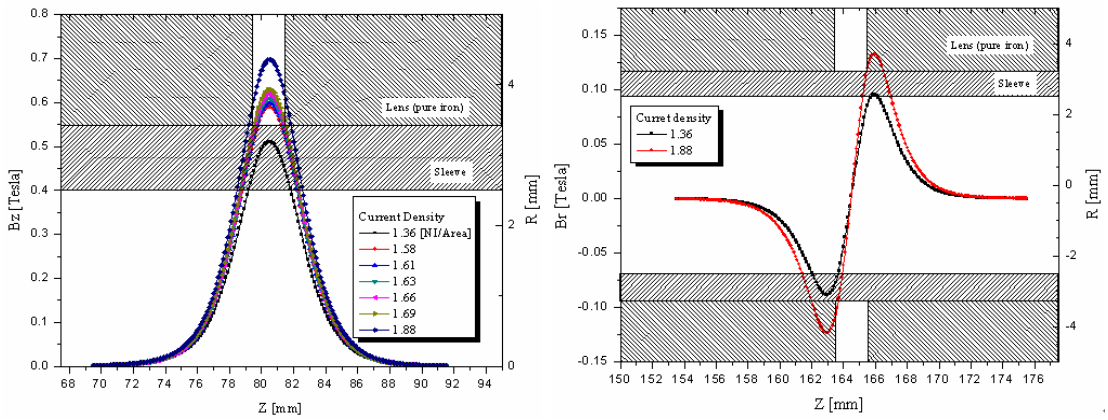

(a) Distribution of the axial & radial magnetic field of the first Condenser lens

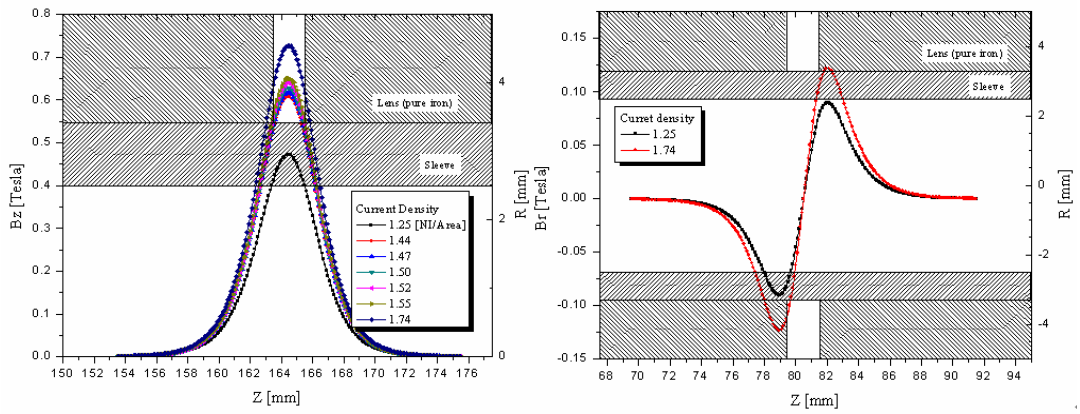

(b) Distribution of the axial & radial magnetic field of the second condenser lens

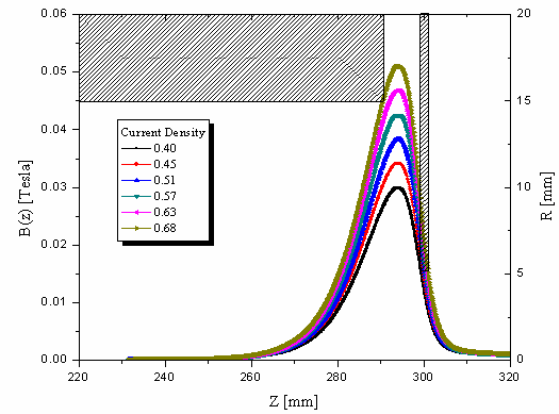

(c) Distribution of the axial & radial magnetic field of the objective lens

Fig. 12. Axial and Radial magnetic field distribution for different excitation current.

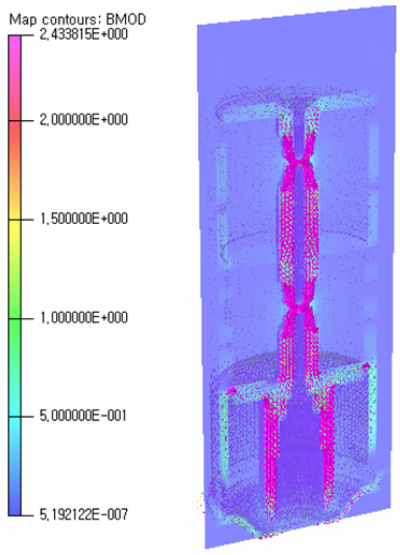

Fig. 13. Distribution of the magnetic potential in the electron optical column.

3.3 Space charge analysis for the electron optical system

OPERA-3D/SCALA was used for the space charge analysis. The first and second condenser lenses and objective lens were added to the analysis model to consider the effect of the magnetic lens, as shown in Fig. 14. The axial length of the analysis domain was set to 320 mm. A finite element mesh was constructed for a quarter section of the model considering the geometric symmetry. An acceleration voltage of 15 kV was applied to the tungsten filament, and a bias voltage of -70 V was applied to the Wehnelt. Fig. 15(a) shows the resulting beam trajectory through the entire column. Fig. 15(b) and (c) show enlarged views of the trajectory around the gun region and the objective lens, respectively. The discharged electron beams were deflected due to the magnetic fields and converged to a specific region having a certain spot radius. Three lenses were modeled to investigate the magnetic flux, which determines the electron beam trajectory. The electron beams were discharged on the tip of the filament (z=-11 mm), and proceeded through the anode and sleeve. Beams that passed into the sleeve hole were refracted due to the magnetic field originating from the condenser lens, and focused to a point at an axial distance of 99.5 mm. The beams then diverged after the first crossover, and converged again due to the magnetic field of the second lens.

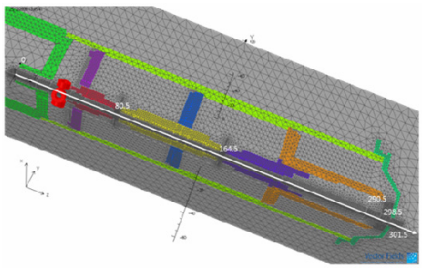

Fig. 14. 3D Model of the SEM column (gun, condenser and objective lens).

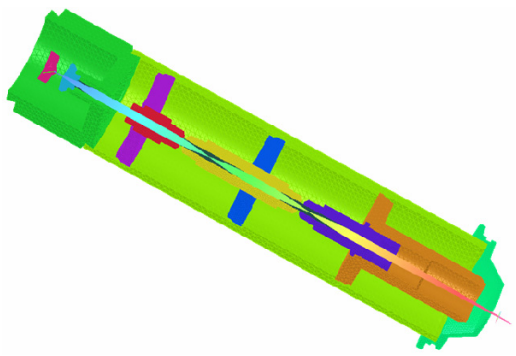

(a) Beam trajectory through the entire column

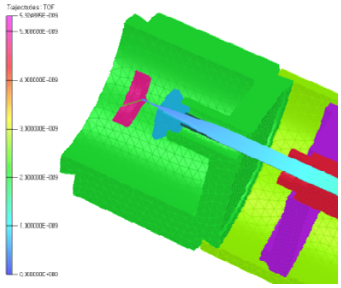

(b) Enlarged view in the gun region

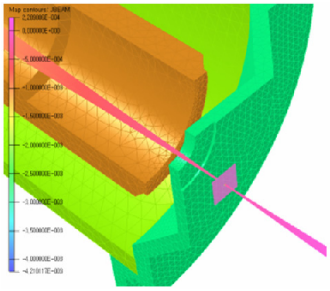

(c) Enlarged view around the objective lens

Fig. 15. Beam trajectory results inside the designed SEM column.

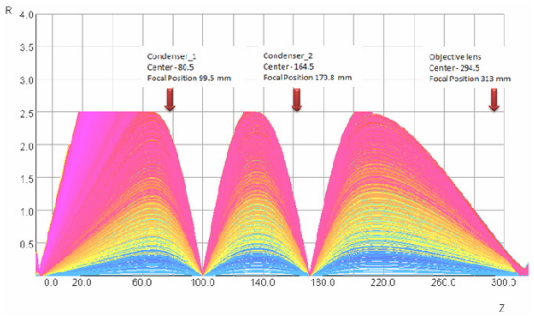

(a) Without apertures

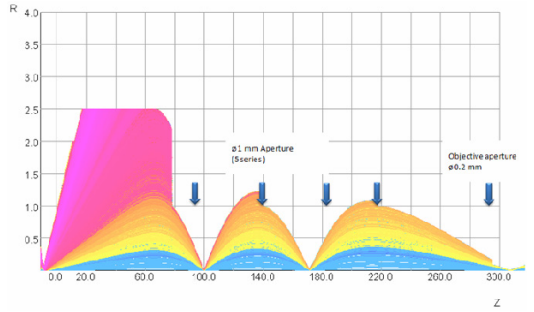

(b) With apertures

Fig. 16. Ray tracing results from the beam source to the image plane (a) without apertures (b) with apertures.

Fig. 16 shows the beam trajectory estimated by solving the ray-tracing equation. Two situations were considered: (a) one without apertures, and (b) one with apertures. The crossover size could be reduced by employing a set of apertures. The emitted beams were refracted and crossed twice due to the magnetic field generated by the two condenser lenses. The first and the second crossing positions corresponded to axial distances of 99.5 and 170.8 mm from the beam source, respectively. The crossover size was small and the aberrations were decreased if apertures were installed between the lenses.

Several aspects must be taken into consideration when designing a high-performance SEM. First, if the distance between two condenser lenses is kept to a minimum, it prevents the electron beam from going out of the center of the lens as long as a sufficient beam current is generated. If the distance is excessively large, then the beam hits an undesirable location, thereby reducing the electron density. Second, to minimize aberration, each aperture diameter must be adjusted to be in the range of 1 mm. Five apertures should be employed to maintain a high resolution. To further improve the resolution, we placed multiple apertures with different sizes inside the long sleeve.

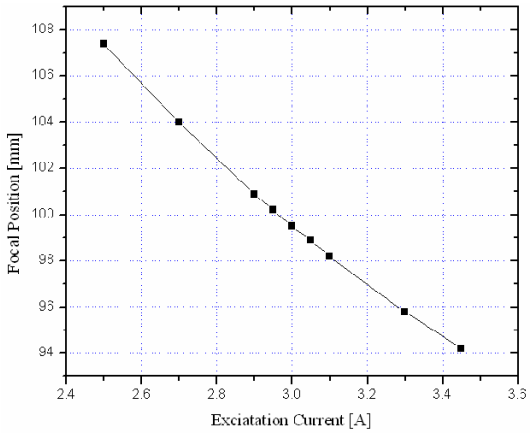

(a) Condenser lens 1

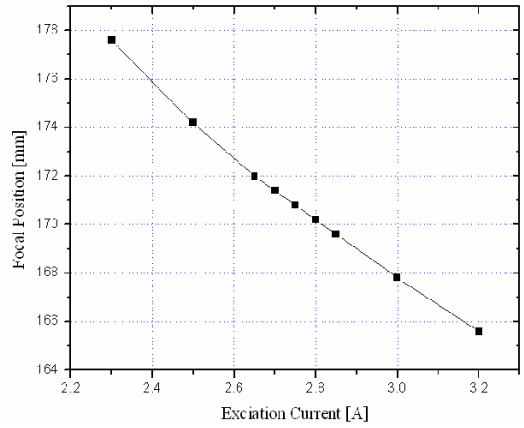

(b) Condenser lens 2

Fig. 17. Focal position for condenser lens 1 (a) and 2 (b).

The inner surface of the sleeve was machined well to have a low surface roughness, minimizing the external interference on the beam trajectory and reinforcing the magnetic field intensity.

An objective lens focuses the beam on the specimen, but it cannot produce an infinitely small spot size due to lens aberrations. Instead it produces a narrow spot that represents a demagnified image of the beam source. The diameter of the spot can be controlled, for example, by reducing the focal length of the objective lens, which results in a spot with a smaller diameter on the specimen. In general, the smaller the spot size, the better the resolution. It becomes increasingly difficult to resolve any two structures whose spacing is less than the diameter of the beam of charged particles. Thus, the spot size is crucial for image quality.

The focal position is proportional to the current supplied to the lens windings. Changing this current density allows the focusing power of the lens to be varied (see Fig. 17). The focal position can be sufficiently varied, meaning that an electron image can be focused by adjusting the lens current.

4. Performance specifications

The performance of the fabricated SEM was verified by observing the specimen images. Test samples of 25- and 100-μm nickel mesh were placed on the specimen holder located in the chamber. Scanned images of the sample are shown in Fig. 18. The ball shaped object could be clearly identified, and the edges of other adjacent objects were also distinctly visible by increasing the magnification and adjusting the focus of the condenser and object lenses.

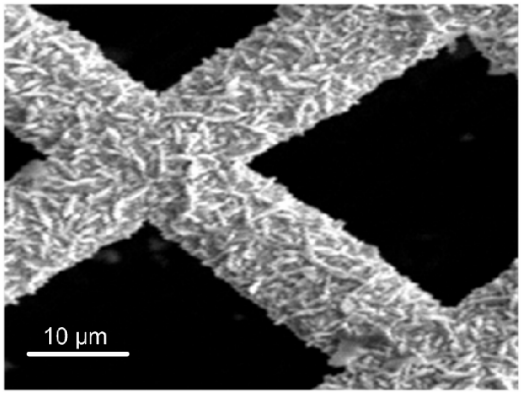

(a) 25 μm nickel mesh

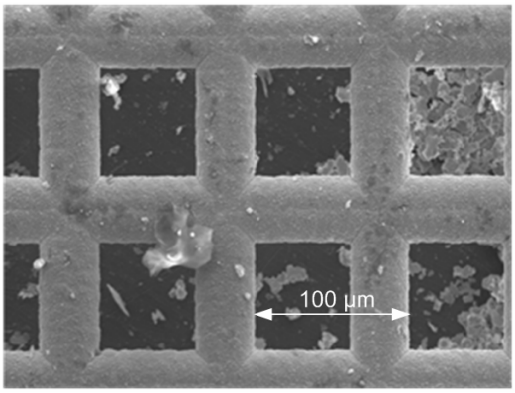

(b) 100 μm mesh sample

Fig. 18. SEM images for a 25 μm nickel mesh sample (a) and 100 μm mesh sample (b).

A high resolution of about 10 nm was achieved. This was estimated from the 6,000× SEM image (image on the left of Fig. 18) at an accelerating voltage of 15 kV. Guided by the simulation results, the dimensions and location of the lenses, apertures, and beam source, and the accelerating voltage were optimally determined for the SEM design and fabrication. These parameters resulted in reduced chromatic aberration, improved beam brightness, even at low-electron probe energies, and reduced beam energy dispersion. When the dimensions or locations of the SEM components were changed, the simulation was able to predict or estimate the beam characteristics very accurately. The detector was able to reliably obtain the amplified signal of the emitted secondary electrons from the specimen. If the acceleration voltage was always stabilized with negligible level of ripples, the SEM image was stable and robust. For our setup, the high-voltage source was fabricated to meet our voltage variation criterion of less than 10^{-3} % ripples, resulting in stable and reliable SEM images. The applied currents on the electromagnetic lenses were about 80 mA; this current was precisely controlled by a 12-bit A/D converter from the digital controller. The applied current to each coil could be more precisely adjusted using our digital controller rather than a conventional analog controller, contributing to a higher-resolution SEM image.

5. Conclusion

A compact thermionic SEM was designed and fabricated, and its performance was tested repeatedly to demonstrate its high performance and stability. After several trials, a high resolution was obtained. The SEM images were stable, which implies that the beam focusing components were fabricated satisfactorily and located appropriately inside the column and chamber. In the design process, the placement and dimensions of the electromagnetic components were analyzed and identified by a finite element simulation using commercial electron beam analysis software (OPERA-3D/SCALA, TOSCA). Computer simulations were successfully used as a design tool to optimize the electron beam motion. The mechanical and electrical parts were optimized through several iterations of experiments and through simulation. Direct and precise measurements of the electron beam trajectory after it passes through the condenser lenses or

object lens are almost impossible, and the dimensions of the lenses and apertures and their location in the column cannot be determined easily. These challenges could be overcome by utilizing finite element analysis. After a SEM is fabricated, strict calibrations of each component are inevitably required to obtain a high-resolution image with extremely small aberrations. We expect that a more precise adjustment of our lenses and apertures, and their optimal placement could further increase the resolution.

We claim that despite being smaller, the performance of our fabricated SEM is on par with other commercial SEMs.

Acknowledgement

The authors would like to thank the support for from the Seoul R&BD program under Grant No. 10583, the Institute of Advanced Machinery and Design at Seoul National University and Grant No. 10011365, funded by the Ministry of Commerce, Industry and Energy.

References

[1] A. Bogner, P.-H. Jouneau, G. Thollet, D. Basset, and C. Gauthier, A history of scanning electron microscopy: Towards wet-STEM imaging, Micron, 38 (2007) 390-401.

[2] W. K. Lo, G. Parthasarathy, C. W. Lo, D. M. Tanenbaum, H. G. Craighead and M. S. Isaacson, Titanium nitride coated tungsten cold field emission source, Journal of Vacuum Science and Technology B, 14 (6) (1996) 3787-3791.

[3] A. V. Crewe, D. N. Eggenberger, J. Wall and L. M. Welter, Electron gun using field emission source, Review of Scientific Instruments, 39 (4) (1968) 576-583.

[4] H. W. Mook and P. Kruit, Optics and design of the fringe field monochromator for a Schottky field emission gun, Nuclear Instruments and Methods in Physics Research A, 427 (1999) 109-120.

[5] R. Y. Lutsch and E. Plies, Initial resolution measurements of miniaturized electrostatic lenses for LVSEM, Ultramicroscopy, 93 (2002) 339-345.

[6] H. S. Kim, D. W. Kim, S. Ahn, Y. C. Kim, J. Cho, S. K. Choi and D. Y. Kim, Arrayed microcolumn operation with a wafer-scale Einzel lens, Microelectronic Engineering, 78-79 (2005) 55-61.

[7] Vector Fields Ltd., OPERA-3D/TOSCA: Reference Manual, 2004.

[8] P. W. Hawkes, Magnetic Electron Lenses, Springer-Verlag, Berlin, 1982.

[9] K. Park, H. Jung, M. J. Park, D. H. Kim and D. Y. Jang, A study on design and analysis for magnetic lenses of a scanning electron microscope using finite element method, Journal of the Korean Society for Precision Engineering, 24 (9) (2007) 95-102.